copy 1/2

UNIVERSITY AT BUFFALO
STATE UNIVERSITY OF NEW YORK

Department of Electrical and Computer Engineering
School of Engineering and Applied Sciences
312 Bonner Hall
Box 601900
Buffalo, New York 14260-1900
(716) 645-2422 ext 1202

sent 1995 February 3
due 1995 February 15
R&T Number: s400024srd
ONR Grant No:N00014-93-1-0483
Grant Period 15 Feb 93 - 14 Feb 96
"High Power Electronics Institute"
RF of SUNY 150-4758A (ONR2b)

SECOND ANNUAL REPORT (Attached)

Effort Period: 15 Feb 1994 - 15 Feb 1995

TO: (3 copies): Scentific Officer Code: 1132P
Gabriel D. Roy
Office of Naval Research
800 North Quincy Street
Arlington, VA 22217-5000

Additional Distribution:
(1 copy): Administrative Grants Officer
Office of Naval Research
Resident Representative N62927
Administrative Contracting Officer
33 Third Avenue - Lower Level
New York, NY 10003-9998

: (1 copy): Director, Naval Research Laboratory
Attn: Code 2627
Washington, DC 20375

: (2 copies): Defense Technical Information Center
Building 5, Cameron Station
Alexandria, VA 22304-6145

FROM: Rich Dollinger
Acting Deputy Director

Richard E Dollinger

COPY: Jim Sarjeant, Principal Investigator
: George Lee, Principal Investigator
: Javaid Laghari, Investigator
: Bonnie Morris, Sponsored Programs
: Travel

ONR2b,"95AY2",006 - Cover Letter -

SECOND ANNUAL REPORT

Effort Period: 15 Feb 1994 - 15 Feb 1995

R&T Number: s400024srd Grant Period: 15 Feb 1993 - 14 Feb 1996

ONR Grant No.: N00014-93-1-0483 Princ. Inv.: Sarjeant and Lee

a. Description of scientific research goals

Develop a physical understanding of the nature of the processes responsible for multistress aging of complex insulation structures, under ac, dc, and pulse conditions, as are utilized in the space environment. This particular environment adds to the general electrical stressing, thermal and radiation aging effects. With the advent of complex high frequency switched-mode power supply and conditioning to reduce weight and volume, today's modern space power systems are increasingly subject to, and must withstand, combined stressing factors not heretofore needing to be considered. In order to understand such multifactor stress aging, and make valid engineering determinations as to practical lifetimes of components, both measurement and signal generation technologies (dc+ac+pulse) not currently available must be developed.

b. Significant results in the past fiscal year

It can be reported that the initial proof of concept and development of a new and novel method to study the aging of insulation structures under high frequency fields (up to 100 kilohertz, typical of most advanced switched mode power supplies) has been successful. The test facility and preliminary data are described in the attached figures. The rationale for undertaking this study was that microelectrical discharge activity is a dominant mechanism that erodes insulation materials, and their interfaces, resulting in reductions in voltage withstand and hence failure. The relationship between such aging and other failure modes as outlined above requires such advanced, and new, diagnostics to assess electrical micropulse activity during high frequency operation of real systems.

Conventional partial discharge detection topologies suffer reduced sensitivity at a rate faster than the frequency increases, rendering them impractical above a few kilohertz. This new high frequency balanced bridge approach yields between 5 and 10 picocoulombs per pulse detectivity at 100 kilohertz, two orders of magnitude more sensitive than any conventional detection technique. This level of sensitivity having been validated, is comparable to 60 Hertz partial discharge detection and will permit traceable comparison of aging rates as a function of frequency, not currently possible any other way. In addition to high frequency ac aging, this year saw successful accelerated dc aging experiments to investigate effects of continuous thermal plus electrical stressing upon the insulation aging. This will provide preliminary complex aging rates and mechanism identification, as well as guidance as to how to proceed with high frequency ac+dc+thermal+radiation insulation aging in a methodical manner. The materials selected were

recommended by US industry and are insulating films presently utilized in numerous space components, namely 10 micrometer thickness capacitor grade biaxially-oriented isotactic polypropylene film. Statistical analysis of the lifetime data included assessment of possible underlying parametric distributions that would support specific assertions as to the fundamental processes responsible for the observed aging. Parametric distributions considered were all of the single failure link class, as this is how these insulation structures are found to fail - i.e., at a single point.

For the range of aging temperatures available (23 to 110 deg C), lifetimes were clearly reduced linearly as the temperature increased, for equal test periods, as well as for the case of fixed temperature and increased test times. This trend correlated quite well with the concentration of atomic oxygen on the film surface, and Young's modulus values. This initial work supports the inference that the growth of microcracks is responsible for weakening of the film both mechanically, and subsequently electrically as crack propagation across the film thickness continues.

In space power systems, the other major insulation issue is the need for reliable cable insulation, particularly to replace polyimide in low to medium voltage power applications wherein moisture is an issue. A study has been undertaken, in conjunction with NASA, of new insulation systems that would include Gore, Tensolite, Filotex, and Teledyne cable insulation system supplied by NASA for evaluation in this part of this research program. Since many of these systems are proprietary formulations at this developmental stage, further materials details will become available over the next short while. These wiring constructions are comprised of rather complex combinations of insulating materials, including but not restricted to, polyimides, teflon and derivatives, and bandings.

The preliminary screening of representative new cabling insulation systems was undertaken via ac, and dc, breakdown measurements. Space-relevant frequencies utilized were 60 to 400 Hertz, allowing comparison with conventional power performance, to the 400 Hertz utilized in many space power systems, particularly for retrofit applications. Temperatures from room to near 200 deg C were applied in a circulating hot air environment.

In general, polyimide insulation showed the highest voltage withstand, decreasing by about 20% at 400 Hertz and 200 deg C. On the other hand, the other insulation systems, operating at lower electrical field stress levels (normally by 50%), were capable of maintaining a stable withstand voltage over the complete range of temperatures, while preserving superior physical properties - flexibility, thermal stability, and surface integrity.

Interaction with industry continues with capacitor manufacturers (Custom Electronics and Aerovox) and developers of specialized transient monitoring apparatus (Mecatronics). Our graduate students continue to interact directly with these organizations as well as with the University of Rochester's Laboratory for Laser Energetics, where one of the largest high voltage pulsed power systems is in the installation stage at this time. We are the external technical advisors to them on pulsed power and insulation issues.

Major Technical Accomplishments for Technology Transfer (Items 1, 2 and 3):

1. Design and Improvement of a Partial Discharge Analyzer for Heightened Detection of Micro-Discharges - Master's Research of C. S. Nowak.

A specialized micro-discharge detection "Partial Discharge Analyzer" has been developed for the HPEI by Biddle Instruments, under prior Government support. Detectability of very small micro-discharges, less than 5 picocoulombs, has proven to be nearly impossible for conventional versions of this apparatus, and not feasible for the research unit subsequently developed for us. An investigation was then undertaken, as a research project, to assess accuracy and suitability of this available system, and possibly areas for improvements.

The limiting factor for all measurements undertaken from signal swamping by the degree of system noise, produced from a variety of sources. A comprehensive system noise analysis was undertaken, and the system noise was characterized, inasmuch as it pertained to its identification and removal. Essentially all noise of significance was traced to magnetic interactions with interlock and control signal lines, from input ac fields coupled primarily through large loop area wiring geometry. Redesigning all of the electronics interconnections, coupled with rerouting of all power and signal lines, resulted in decreasing the system noise by a factor of 20 times, down to 10 picocoulombs. The present detectivity level of 5-10 picocoulombs is more than adequate for experiments over the next two year time period. Further reduction, down into the < 0.5 picocoulomb level, will be necessary for future high resolution experiments in the next phase of this high power electronics program.

All these enhancements to performance have been made available to U.S. industry, mainly through site visits to the institute during 1994. They are being incorporated into at least one research class partial discharge detection system, being upgraded by Custom Electronics Incorporated.

2. Characteristics of Partial Discharge Detection in Preparation for Assessing Applicable Data Acquisition Technology - Master's research of J. W. Stewart.

The above micro-discharge detection system is widely used in industry for quality control and diagnostic testing to provide data as to a product's suitability for use under high ($>>$ 100 volts) voltage conditions. Detection and acquisition methods have reached a point where automated acquisition is needed to achieve necessary further accuracy in performance assessment. This research concerns itself with the instrumentation of the micro electrical discharges and the capability and reliability of the signal processing circuitry in the detection system. In particular, an assessment was undertaken of high pass filters, analog-to-digital converters, wide-band amplifiers, and electronic data collection techniques used in the analysis of micro-discharge signals.

The results of this work was a thorough summary of existing mature technology as used for micro-discharge detectors, followed by development of concepts for real-time data acquisition systems for on-line system performance analysis. In essence, it was determined that multimegahertz flash analog-to-digital signal acquisition is an acceptable minimum capability for next generation systems. At this point in time, this is not yet available to meet the refresh rates that are driven by actual micro-discharge trains in systems. It is noted that next generation digitizing systems to meet these needs remain commercially several years away, although new digitizing oscilloscopes recently introduced by Hewlett Packard provide nearly the required capability but at a cost far higher than that of the original Biddle complete system. For commercial applications, in interacting with visiting companies, we were told added costs such as this were too prohibitive. Consideration is being given to develop a miniaturized flash conversion system, in conjunction with U.S. industry. Discussions are underway.

3. High Speed Linear Motor Design - Master's research by D. J. Foley

High speed linear motor systems are under consideration for fast electro-mechanical actuator use in space and land applications, to displace hazardous and temperature sensitive hydraulic fluid systems. Essentially, a linear motor consists of either a conductor that is free to move through a permanent magnet along two conducting strips that electrically connect the machine to an external energizing circuit, or a permanent magnet that can move with respect to this conductor. The construction is such that the magnetic field, conductor motion, and current flow are mutually perpendicular.

This specific project was to design and validate submillisecond response linear motor topologies that are operated by man-rated voltages (i.e., < 600 volts), with unconditionally protected energizing capacitor banks. Successful sabot acceleration to > 500 m/s were achieved.

The other major application for this technology is for hypervelocity mass acceleration, particularly for mass-to-space, and related applications. Transition of these new power conditioning technologies to industry is just underway and is expected to be completed in 1995.

c. Plans for next year's research

The comprehensive insulation aging methodology and engineering scaling studies initiated this year must be continued, with emphasis upon materials of relevance to the space environment. In addition, materials utilized in land and underwater systems will be assessed as is practical in order to validate the scalability of the approaches undertaken, and identify any changes in aging in these other related environments that are also of interest to industry and the Navy. Actual space components will be used in place of insulation media to anchor the relevance of these aging approaches to actual device level components. Of particular interest is the aging under dc+ac conditions, representative of the majority of new space, land, and underwater power system environments.

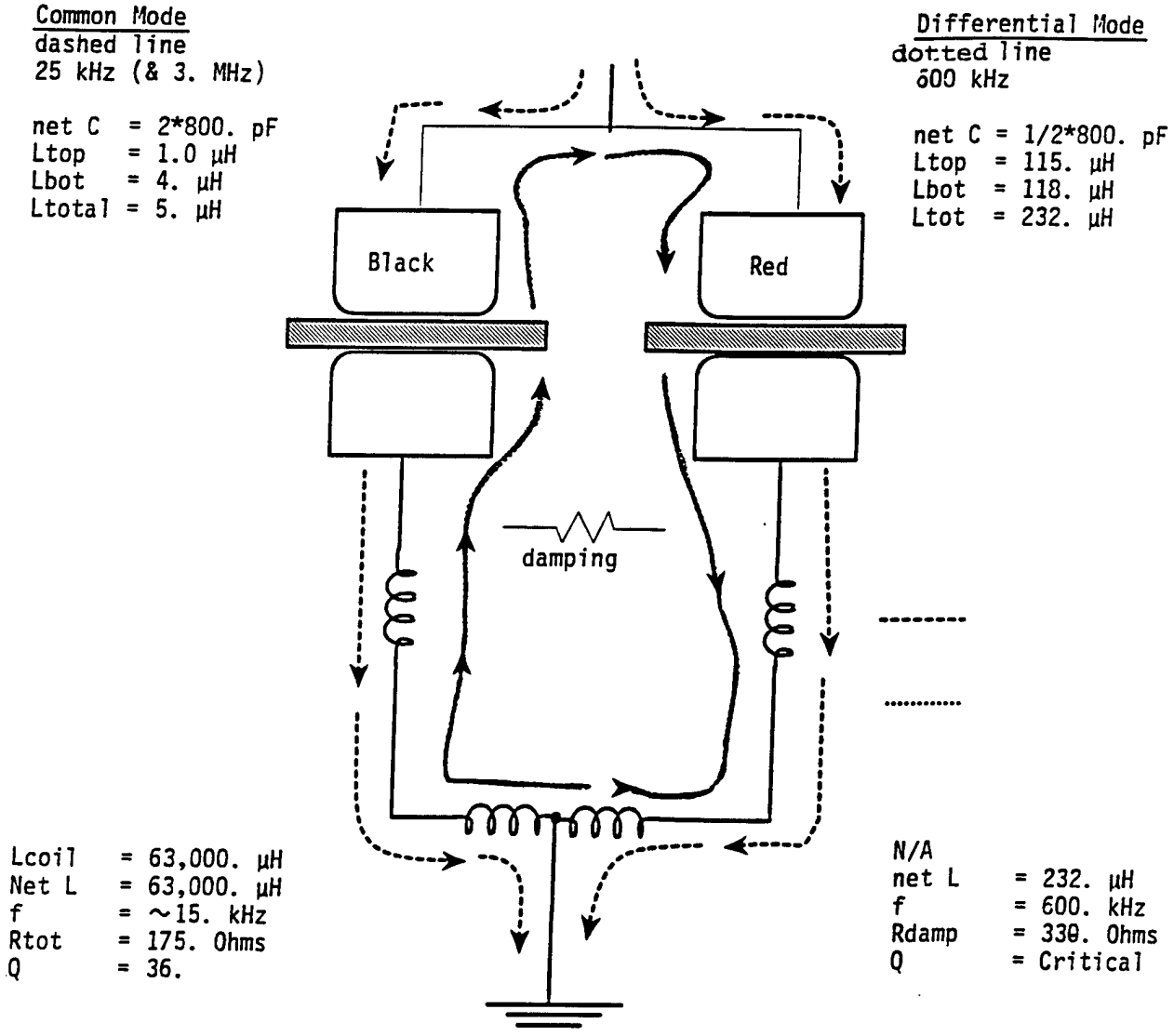

Figure 1. Schematic of torroidal bridge test fixture. Long dashes represent the current flow caused by the applied test voltage. This current should divide, with equal amounts going through each branch. The solid line represents the current path generated by a discharge event. Note that the mutual coupling associated with each torroid opposes for the common mode current and adds for discharge current. The values shown represent measured values of the components as described in chapter III for both common mode and differential mode arrangements.

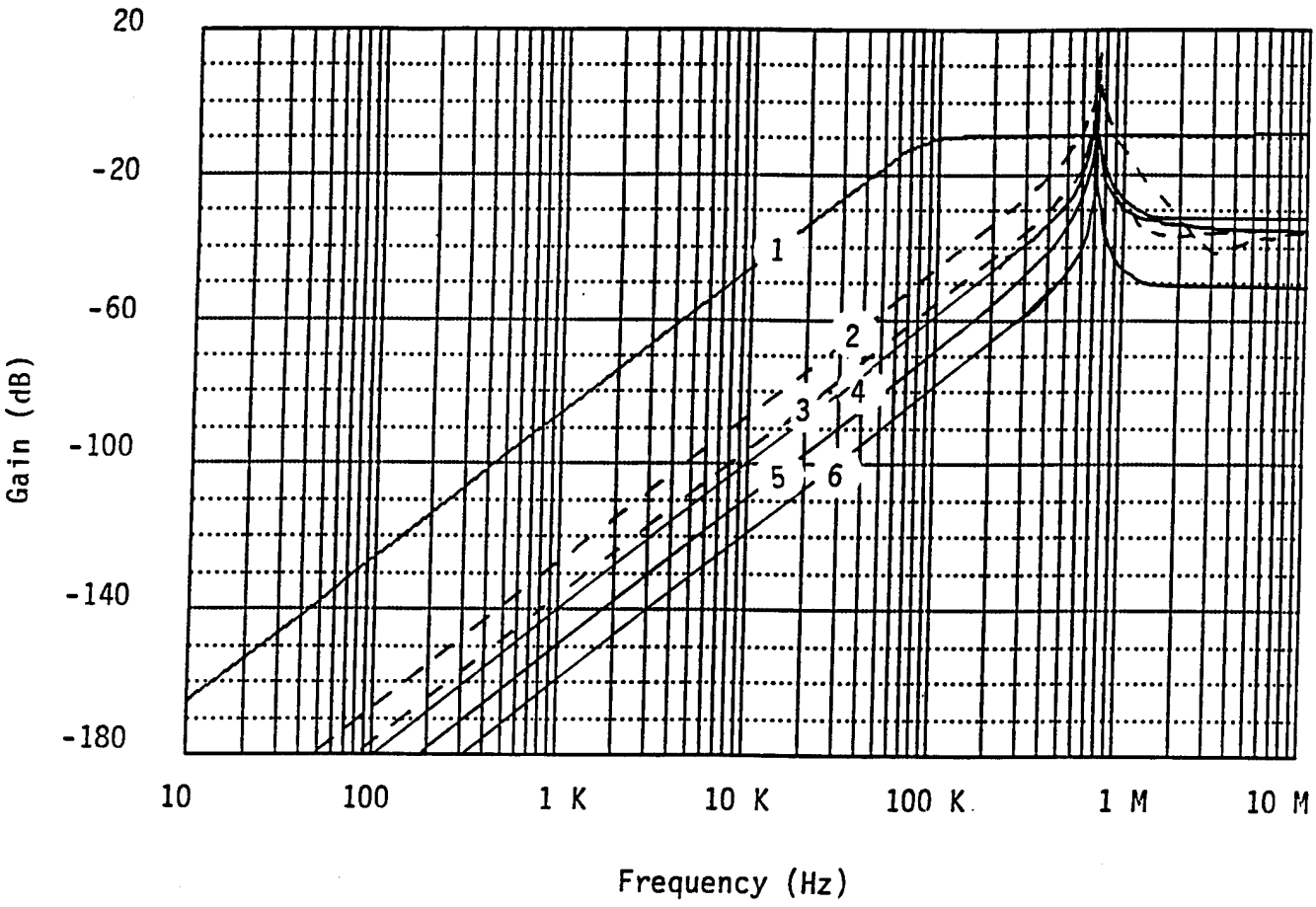

Figure 2. Bode plot generated from Microcap III ac analysis. Simulations include 1) conventional PSF of Figure II-4 for comparison, 2) measured values of toroids w/50% variation in sample capacitance, 3) measured values of toroids w/10% variation in sample capacitance, 4) 10% simulated variation of toroids with matched capacitance, 5) measured values of toroids with matched capacitance, and 6) 1% simulated variation in values of toroids of matched sample capacitance. All cases show substantial improvement in filtering over conventional method.

LIST OF REFEREED PUBLICATIONS

Attachments:

1. J. Stopher and R. Dollinger, "An Innovative High Frequency Microdischarge Detection Technique," Conference Record of the 1994 IEEE International Symposium on Electrical Insulation, Pittsburgh, PA, June 5-8, 1994, pp. 237-240.

2. A. N. Stokes, J. R. Laghari and W. J. Sarjeant, "Comparative Statistical Studies of Aging Models for Polypropylene Films," Conference Record of the 1994 IEEE International Symposium on Electrical Insulation, Pittsburgh, PA, June 5-8, 1994, pp. 332-335.

3. A. N. Hammoud, M. W. Stavnes, J. L. Suthar, W. Khachen and J. R. Laghari, "Testing of Cable Insulation for Aerospace Application," Conference Record of the 1994 IEEE International Symposium on Electrical Insulation, Pittsburgh, PA, June 5-8, 1994, pp. 174-177.

4. C. Nowak, J. Stopher, J. Zirnheld and R. Dollinger, "Microdischarge Detection in High Frequency Capacitors," Conference Record of the 1994 Twenty-First International Power Modulator Symposium, Costa Mesa, CA, June 27-30, 1994, pp. 252-255.

DEGREES GRANTED

1.	C. Nowak,	June	1994	Master-of-Science
2.	J. Stopher,	September	1994	Doctor-of-Philosophy
3.	J. Stewart,	May	1994	Master-of-Engineering
4.	S. Sheeshia,	September	1994	Master-of-Engineering
5.	F. Silvernail,	September	1994	Master-of-Engineering
6.	D. Foley,	December	1994	Master-of-Engineering
7.	G. DelVecchio,	December	1994	Master-of-Engineering
8.	E. Gutierrez,	December	1994	Master-of-Engineering

Conference Record of the 1994 IEEE International Symposium on Electrical Insulation, Pittsburgh, PA USA, June 5-8, 1994

An Innovative High Frequency Microdischarge Detection Technique

J. Stopher and R. Dollinger
312 Bonner Hall
University at Buffalo, SUNY
Buffalo, NY 14260

Abstract

Today's modern electrical devices are increasingly subject to, and must withstand, high frequency stressing. Such stressing contributes to accelerated aging of electrical insulation and has resulted in premature failure of components. In order to understand the aging mechanisms (i.e. erosion) and make valid conclusions regarding the service lifetime of components used under high frequency conditions, the electrical insulation must be examined under the same high frequency conditions as that it will be used. Conventional electrical techniques used to detect partial discharges are limited to below 2 kHz applied ac test voltages. In order to stress electrical insulation and examine the microdischarge activity for frequencies up to 100 kHz, a new technique was developed. This technique uses series resonance to achieve high frequency sinusoidal steady state ac test voltage and a bridge type test cell to detect the resulting microdischarge activity. Calibration and simulations support the critically damped single output pulse per discharge events temporal resolution of <.5μs. Typical output traces are presented and preliminary test data is presented.

Introduction

The increased use of high frequency components are evident in such applications as radar modulators, switching supplies, and computers. There have been instances where entire projects have been set back due to early failure of capacitors, which resulted from use under conditions which the designed service life was not completely understood. There has been much work to classify the physical mechanisms which contribute to the failure of the insulation systems subject to such stresses and which are accelerated under higher frequencies. Microdischarge activity is a dominant mechanism that erodes the insulating material and results in failure, but the relationship between aging caused by these discharges and other failure modes (i.e. thermal runaway) requires advances in diagnostics to provide discharge activity data during high frequency stressing.

This work was partially supported by BMDO/ONR grant # N00014-93-1-0483.

Conventional filter techniques use an LCR circuit that is shock excited by discharge events and output a single voltage pulse proportional in magnitude to the size of discharge. However, the voltage drop across the LCR network, also called the detection impedance, increases with increasing frequency. Because of this, a portion of the test frequency voltage is output with the discharge signals and reduces the facility's ability to perform low level measurements. In general, this conventional method is acceptable for test frequencies under 2 kHz.

Design and Development

Test Facility

The test facility, shown in Figure 1, is comprised of a series resonant supply, bridge-type test fixture, detection transformer, filter, shielding, fault protection, measurement apparatus, and calibration circuitry.

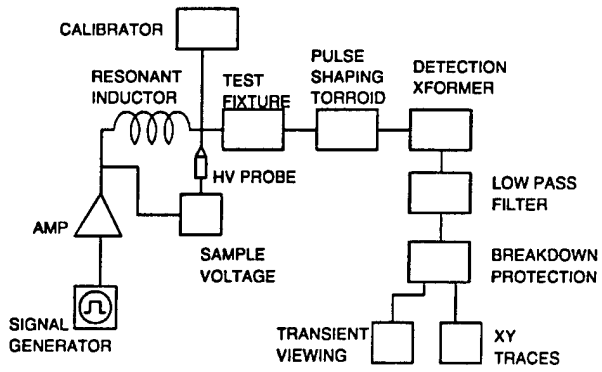

Figure 1. Major components of facility.

High Voltage Supply

A series resonant technique was chosen to generate the partial discharge free high voltage steady-state sinusoidal ac test frequencies between 2 kHz and 100 kHz, across capacitive test objects. Series resonance was achieved with the test object capacitance, a hand wound air core inductor, an audio amplifier, and a signal generator.

Series resonance provides desirable characteristics; it limits the amount of energy available in the event of sample failure, as a result of sample failure, the capacitance is changed sufficiently to drop out of resonance thereby reducing peak voltages, and finally, the current draw decreases off resonance allowing easy control while adjusting test frequency.

A Hewlitt Packard 651B test oscillator and a 100 watt (~90 Vpp) with 50 Ω output impedance was used to generate the applied test voltage. The primary inductance used for resonance was provided by either single layer hand wound air core inductors, which ranged from 40 μH to 60 mH, or by a commercially wound components such as a Brooks coil (5 H) or other power transformer secondaries (~2H). The available inductors, together with typical test object capacitance on the order of 2000 pF, provided resonant test frequencies between 2 kHz through 100 kHz by virtue of the following equation;

$$\omega_o = \frac{1}{\sqrt{LC}} \qquad [1]$$

The available resonant frequencies actually went well beyond 1 MHz, however the response of the audio amplifier dropped off above 100 kHz.

A Gentec 10,000:1 20 kV partial discharge free high voltage probe was used to observe the test specimen voltage. This capacitive probe has less than 20 pF and did not significantly load the specimen. While the specimen voltage was monitored at low voltage, the signal generator was manually adjusted until resonance was observed by a peak rise in voltage. The peak voltage can be estimated by multiplying the applied voltage and the quality factor Q of the series resonant circuit, given by;

$$Q = \frac{\sqrt{L/C}}{R} \qquad [2]$$

The inductors, capacitance, and amplifier used provided a Q on the order of 25, and generated test voltages near 2.5 kV.

Test Fixture

The test fixture, illustrated in Figure 2, provides the basis for allowing high frequency microdischarge detection. It consists of two specimen cells, a pulse shaping toroid, a detection transformer, and a damping resistor.

The two pairs of 2" diameter brass electrodes conform to ANSI standards. Both test objects are charged simultaneously. The charging current travels through each branch of the pulse shaping toroid, through the detection transformer primary, out the center tap, and back to the power supply.

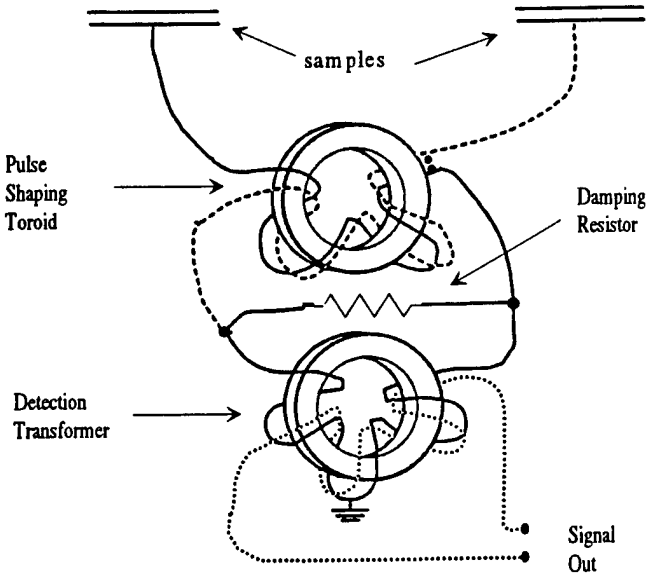

Figure 2. High frequency bridge type test fixture.

The winding sense around both toroids in each branch of the test fixture is counter with respect to each other. This opposing sense reduces the inductance and subsequently provides a minimum impedance path for charging. More importantly, a minimum net flux is generated within the transformer core, and therefore, minimum output noise is generated at the secondary. In fact, if the currents in each branch are equal, and the number of turns about each branch of the transformer is equal, then there should be zero output, regardless of frequency or voltage. The N*I forces which generate the flux are illustrated in Figure 3. Note that this effect is true for charging currents (common mode currents) and an opposite effect (maximum voltage out) for currents originating within the specimen test cells.

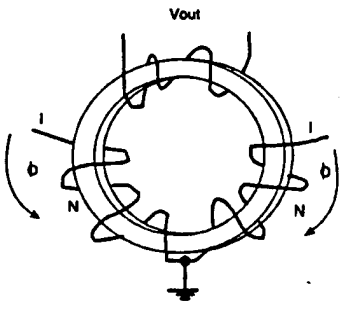

$$V_{out} \propto N_s\phi \propto N_s(N_{p1}I_1 - N_{p2}I_2)$$

*Figure 3. N*I forces that generate core flux which creates the output at the secondary.*

Discharge Event

During a discharge, the voltage generated by charge recombination distributes itself around the path of the test fixture, primarily by inductive distribution. The resulting current flow is confined to within the test fixture and circulates through the detection transformer. This effect is assured because the test fixture impedance is small compared to that of the resonant inductor and power supply. Initially, the current will flow until the charge on both specimens distributes evenly. The resulting transient response is a critically damped single pulse waveform caused by the parallel RLC network of the fixture and is described analytically and by computer simulations. Control of the pulse shape and duration is accomplished by changing the inductance of the pulse shaping toroid and the damping resistor.

The pulse shaping toroid performs two functions. It increases the differential mode (discharge current path) inductance to help define the resulting transient signal waveform. The total inductance should be large enough that the transient duration lies above the test frequencies (> 100 kHz) and below the higher sub harmonics and other noise (< 5 MHz). This relatively large inductive path allows the LCR network to be critically damped (i.e. if L is too low, the response will ring). Secondly, the pulse shaping toroid reduces part of the discharge signal. This safety feature prevents sensitive equipment connected to the output in the event of sample failure however does reduce the microdischarge detectivity.

The output stage of the secondary of the detection transformer connects to a low pass filter with a 1 MHz cutoff. Although this filter decreases the magnitude of output response for the high frequency discharge events (by about half), any spurious noise and high frequency sub harmonics are severely attenuated. Four diodes (two each way) provide protection to the oscilloscopes in the event large voltages occur, as in sample breakdown. For the diodes to turn on and short the output, a discharge on the order of 7,500 pC sample discharge would have to occur - far higher than normal microdischarge activity detection needs require.

Measurements

Typical output of the facility were observed and measured to characterize the facility's minimum detectivity and linearity. These transient voltage traces were created by a new calibration technique developed for this detection technique and will be covered in detail in future publications. Figure 4 shows transient voltage responses from two calibration pulses.

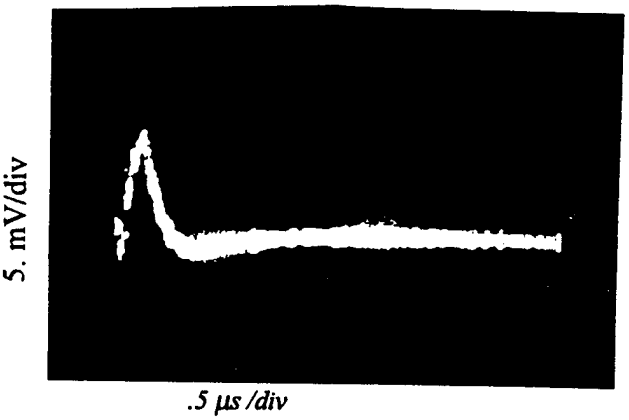

Figure 4a. 98 pC calibration pulse transient response.

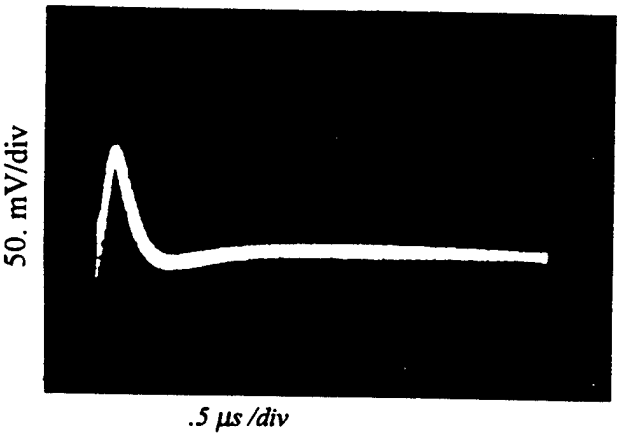

Figure 4b. 884 pC calibration pulse transient response.

Note that the transient response is a single pulse and is near critically damped for each observation and is about .11 mV/pC. The consistent magnitude and transient waveform suggests the technique is linear and its consistent single pulse response allows interfacing with standard diagnostic equipment normally used with conventional discharge detection techniques such as pulse height analyzers.

Discharge Signal Display

Discharge events are observed at the output by several methods. The first method is a time domain signature of microdischarge activity. The transient voltage waveform created as a result of a discharge is viewed on an oscilloscope with storage capability. Figure 5 illustrates individual discharge generated voltage wave forms. This particular trace indicates discharges occurring in each cell because of both polarities being present. The output signal of this method is usually connected to a pulse height analyzer for counting and logging pulse events over long periods of time. The signal trace in the photograph of Figure

6 is the superposition of the output waveform and the attenuated test voltage; this method is used to help identify the phase in which the activity takes place.

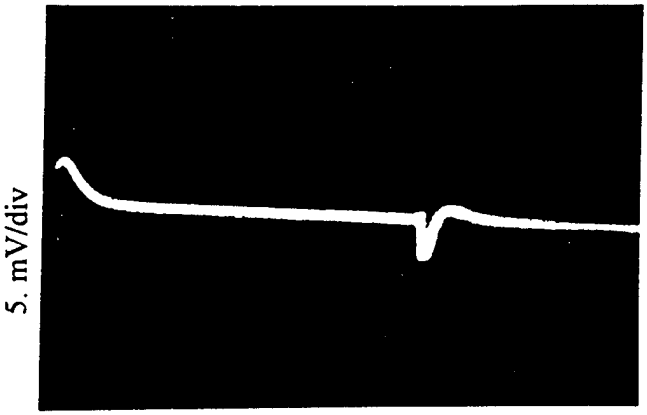

Figure 5. Photograph of individual transient discharge signal voltage traces. Clearly, the discharge activity is originating from opposite electrode pairs.

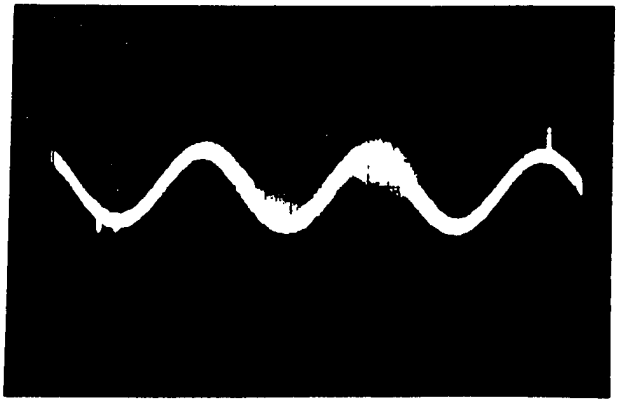

Figure 6. Transient voltage traces of discharge activity superimposed on top of the applied test voltage. 10 mV/div discharges on 500 V/div main.

Discharge activity also can be viewed in an elliptical trace which allows identification of discharge activity regardless of applied frequency.

Preliminary Results

The ubiquitous relationship between time to failure and applied voltage, identifies ranges of the dominant failure mechanisms as a function of time. Generally, this relationship is broken into lose regions of dominating failure mechanisms such as intrinsic, thermal, and erosion. At high frequencies, this relationship is much less understood and the mechanisms may be less dominant and more related. This preliminary test examined candidate thin film capacitor grade insulation time-to-fail versus frequency and observed the microdischarge activity during the aging process to look for evidence of the interaction between microdischarge erosion and other processes.

Eight micron polypropylene (PP), submersed in Flourinert, was stressed at 530 Vrms, at sinusoidal frequencies, between 2 - 100 kHz. The Flourinert was used to minimize the external surface discharge activity and constrain the failure mechanisms to characteristics of the insulation material. The time-to-breakdown was recorded for a minimum of seven samples (results provided in Figure 7), and microdischarge activity observed during the aging process.

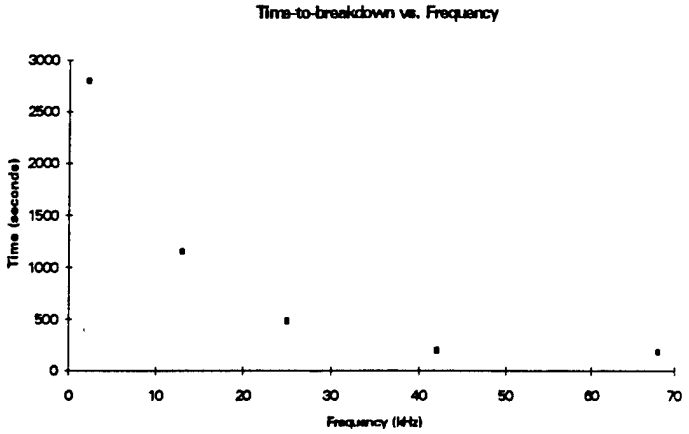

Figure 7. Time to breakdown data for preliminary test of 8 micron polypropylene submerged in Flourinert at 530 Vrms.

An important observation during this test, was the absence of any significant discharge activity during stressing of the insulation specimens until the moment immediately preceding catastrophic failure. This suggests that the dominant aging mechanism is not entirely erosion.

Conclusion

A new technique to stress capacitive samples and detect microdischarge activity under high frequency sinusoidal steady state high voltage conditions was developed.

Future work will include futher investigation of insulation under a wide range of temperature controlled conditions to help determine the role of thermal characteristics in aging and to more conclusively and quantitatively document the microdischarge activity during the aging process. In addition, capacitors will be used in place of the test fixture's insulation specimen cells to prove the utility in examining device level components.

Conference Record of the 1994 IEEE International Symposium on Electrical Insulation, Pittsburgh, PA USA, June 5-8, 1994

COMPARATIVE STATISTICAL STUDIES OF AGING MODELS FOR POLYPROPYLENE FILMS

A. N. Stokes, J. R. Laghari and W. J. Sarjeant

Department of Electrical Engineering
State University of New York at Buffalo
Buffalo, New York

Abstract

Accelerated aging experiments are conducted to investigate the effects of continuous thermal aging on the DC electrical lifetimes of capacitor grade biaxially-oriented isotactic polypropylene film. Statistical analysis of the lifetime data includes assessment of possible underlying parametric distributions such as the 2-parameter Weibull (*weakest link time-to-failure*) and the Lognormal (*cumulative damage time-to-failure*) distributions via graphical, analytical and residual analysis. Parametric and Nonparametric methods are used. The mean life is fitted into semi-empirical (quasi-theoretical) models available in the literature to describe the behavior of the film within the stress range tested. Multiple-linear regression is used to compute parameters of the life-stress models. A thorough regression analysis including goodness of fit measures such as (χ^2) and (R^2) is carried out using the SAS package.

Introduction

Aging studies are needed to understand and model the behavior of insulation systems under sequential and simultaneous accelerated stresses. The high variability in the data necessitates the collection of a large amount of data and the use of statistical methods for summary and analysis.

Statistical analysis/inference deals with estimation and hypothesis testing using a finite set of sample data. An interval estimator is more appropriate and realistic than a point estimator. It consists of a range of error around the point estimate which is a function of the sample statistics and the spread of data defined by the confidence interval. The larger the number of samples, the narrower the interval and the more accurate the point estimate. Hypothesis testing involves 1) defining the null and alternative hypotheses; 2) choosing a significance level α, at which there is a $(1-\alpha)$x100% chance of selecting a random sample that will produce an interval containing the parameter; 3) selecting an appropriate test statistic (parametric or nonparametric) along with critical regions (acceptance/rejection bands; and 4) deciding to reject/accept the null hypothesis based on the computed value of the test statistic and the critical regions (or the P value which defines the minimum level of significance).

A plethora of statistical methods is available for lifetime data analysis of insulation systems many of which are implemented here using the SAS software package [1]. Areas of analysis are: 1) *Data check and summary*: outliers, influential data, violations of assumptions about heterogeneity or independence of errors, and summary into a few meaningful parameters representing average life and the inherent variability; 2) *Goodness of Fit with candidate distributions* such as the Lognormal and the Weibull; 3) *Analysis of variance* to study effects and possible interaction of the independent variables (stresses); 4) *Estimation of Model/Distribution of the stress-life relationship via regression* (empirical curve fitting) along with choice of most significant among investigated, keeping in mind that the statistical conclusion may not be a scientific one and that no model is completely correct but is merely a useful tool describing some aspects of the system observed. Graphical and analytical (using parametric and nonparametric techniques) methods augment each other for each step of analysis.

In this paper a multitude of statistical methods are implemented to analyze the results from the study of accelerated thermal pre-aging of polypropylene films, details of which are given in the following sections.

Experimental Details

A study of the effects of continuous thermal aging in circulating air at two temperatures (90°C and 110°C) for two time periods (300hrs and 500hrs) on the DC electrical lifetimes at room temperature of polypropylene films is conducted. The four conditions comprise the four treatment groups, the lifetimes of which are compared with those of the control samples. All five sets used randomly selected samples of polypropylene film (25μm thick) of the same geometric size. Ten replicate measurements of lifetimes and breakdown voltages were taken at each of four electrical stress level (16kV, 15kV, 14kV, and 13kV). The lifetime data from the accelerated tests are complete and exhibit high scatter as expected due to possible local microscopic defects that vary from sample to sample.

Statistical Details and Results

Graphical Techniques though subjective, offer a variety of simple preliminary methods using both lifetime data and residuals that provide insight into various aspects of the data. Lifetime data fit to a distribution at a given stress level is checked by using probability plots. Ordered failure time data is ranked to estimate an empirical cdf using plotting positions such as: 100(i/n), 100i/(n+1), 100(i-.5)/n or 100(i-.3)/(n+.4). These are all equivalent as long as they are used consistently [2]. Reasonably linear plots suggest adequacy of the corresponding probability distribution and parallel lines at different stresses indicate similar shape parameters (failure mechanisms). Fig. (1) shows the Weibull and Lognormal probability plots of the lifetimes of the polypropylene samples heated at 110°C for 500 hours using the median plotting positions; 100(i-0.3)/(n+0.4). The plots show reasonably straight lines on both plots suggesting their equal validity. The $(1-\alpha)$x100 CI bands show a range of error around the estimated parameters and serve to compare significant vs. nonsignificant (overlapping) differences. However, this is a misleading technique since it is a function of the number of samples used. Plotting the pooled residuals (raw or standardized) on the probability plot provides a final check on the validity of the distribution.

Graphical techniques are also used for detecting outliers (data-points that deviate appreciably from the bulk data) and checking for heteroscadasticity of variances and correlation (nonindependence) of errors, all of which can lead to misleading results and invalid inference. Plots of residuals vs. each variable in a given model and vs. the response provide a final check on the appropriate models for the stress-life behavior.

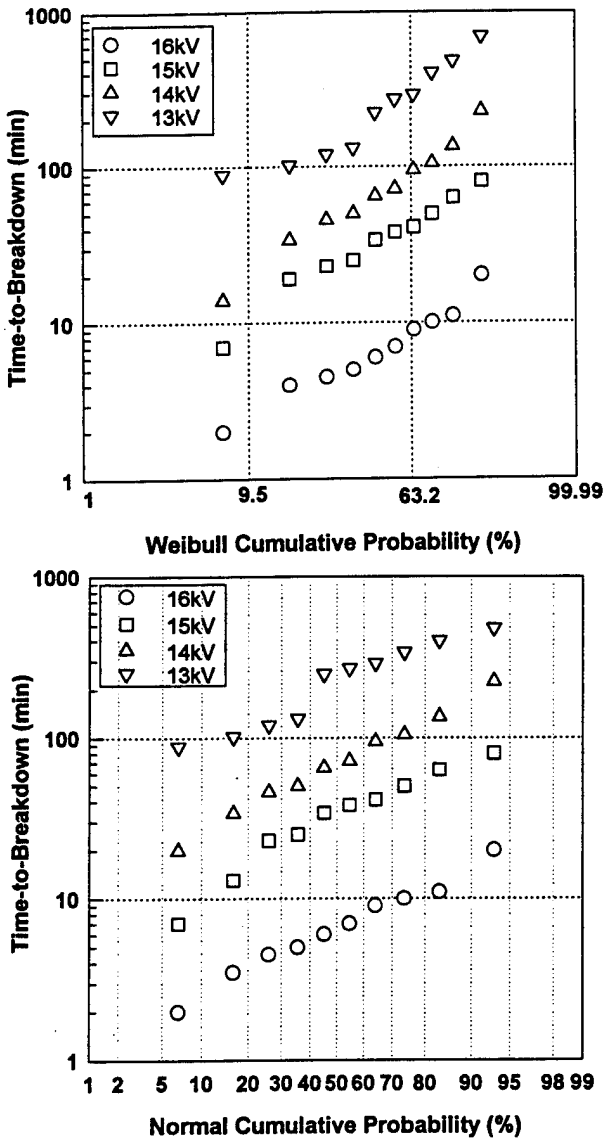

Figure 1: Weibull and Lognormal probability plots of the lifetimes of thermally aged (@ 110C for 500 hours) PP films

Analytic techniques compute a test statistic (parametric or nonparametric) from the available data and compare it to a critical value which is a function of the number of samples and chosen level of α, to test a hypothesis. Parametric methods use test statistics that are functions of the assumed parametric distribution of the data. Nonparametric (distribution free) methods compute test statistics that are functions of the ranks of the response variable rather than its actual values. The location parameter is usually the median.

Some of the nonparametric tests for goodness of fit are: The K-S. (Kolmogorov-Smirnov) test statistic test for K samples [3], Lillifors test for Normality [3], The Wilk-Shapiro, W test for normality and the Shapiro-Brain; a modified W test for the Weibull distribution.

Table I gives values of the computed test statistics for the lower tailed W and the two tailed Shapiro-Brain tests along with the rejection bands at α=0.1. The values indicate insufficient evidence to reject either as a valid underlying distribution for the lifetime data supporting the graphical analysis.

Table 1: Computed values of the Wilk-Shapiro, W test (critical value: 0.87) and the Shapiro-Brain, W' test (critical range: 0.35,1.04) @ 0 1 level

Samples| Voltage	13kV	14kV	15kV	16kV
Control	W=0.97 W'=0.83	W=0.95 W'=0.78	W=0.98 W'=0.74	W=0.97 W'=0.70
Treated @90C/300hrs	W=0.98 W'=0.81	W=0.98 W'=0.79	W=0.97 W'=0.70	W=0.96 W'=0.78
Treated @90C/500hrs	W=0.97 W'=0.68	W=0.99 W'=0.91	W=0.98 W'=0.79	W=0.97 W'=0.80
Treated @110C/300hrs	W=0.98 W'=0.75	W=0.97 W'=0.77	W=0.93 W'=0.56	W=0.93 W'=0.56
Treated @110C/500hrs	W=0.95 W'=0.89	W=0.99 W'=0.96	W=0.95 W'=0.81	W=0.98 W'=0.86

For data analysis, outliers are checked by standardized residuals whose values are greater than 2.50, Cook's D statistic, influence statistics for observations that cause inflation in variance and Press residuals [1]. Two data points were detected as outliers, however they had no significant effect on the estimated parameters.

Characteristic Lifetimes and Trends

Both the Lognormal and the Weibull distributions appear indistinguishable with small sample sizes and either is sufficiently valid if one's only interested in a location parameter to summarize the data and obtain an average life at a given stress. Table 2. shows the Weibull Characteristic life=63.2 percentile along with 90% CI using reference [4]. A general increase in lifetime is noted for the thermally treated samples as compared to the control. Such an observation is expected as thermal energy serves to increase the order of the long polymer chains increasing crystallinity and consequently the strength of the film. Thermal aging at 90°C for 300 hours is seen to increase the lifetime of the film, however, the trend is reversed with increased treatment hours to 500 hours or increased temperature to 110°C. The significance of these observations is tested by Analysis of Variance.

Table 2: Weibull Characteristic Life and 90% Confidence Intervals for aged and unaged Polypropylene films

Sample/Voltage	13kV	14kV	15kV	16kV
Control	307.7 (205.0,468.0)	70.9 (50.2,101.0)	24.7 (17.9,34.4)	5 (3.7,7.0)
Treated @90C/300hrs	1050 (646.0,1731.0)	595.2 (360.0,1000.0)	96.9 (61.0,157.3)	8.8 (5.1,15.4)
Treated @90C/500hrs	501.7 (324.0,786.4)	176.4 (107.8,293.3)	44.6 (29.0,69.5)	7.6 (4.8,12.2)
Treated @110C/300hrs	378.2 (270.8,533.2)	112 (74.0,171.3)	60.6 (36.7,101.6)	13.2 (9.0,19.6)
Treated @110C/500hrs	314.4 (211.6,472.8)	95.7 (64.6,143.7)	43.7 (32.0,60.1)	8.7 (6.2,12.3)

ANOVA

Analysis of Variance partitions the total variation in the response variable into systematic components due to regression variables and a random component due to error. The R^2, multiple correlation coefficient, indicates how much variability is due to regression variables vs. chance (error). An F test assesses the effects of individual stress variables (main effects) on the response

variable and any interaction between them (secondary effects) assuming a (log)Normal distribution. Analysis of Means, ANOM for multiple comparisons between group means allows the separate analysis of which means are different using measures such as Tukey's HSD (Honest Significant difference). Fig. (2) is an annotated output from SAS procedure ANOVA.

The three-way ANOVA at a (0.1) level shows that voltage has the largest effect on the lifetime, followed by treatment time and treatment temperature. Interaction among voltage and treatment temperature followed by interaction among treatment temperature time are the only significant interaction terms. An R^2 of 0.80 indicates that the three stress variables account for 80% of the variation in the data. By arranging the lifetime data into five groups and performing a one-way classification, the ANOM indicates a significant difference between the control group and treated groups across all voltage levels. Among the treated groups there is some overlap.

The nonparametric equivalent of the ANOVA is the Kruskal-Wallis for k mutually independent samples drawn from continuous populations with unknown medians [4]. The SAS procedure Npar1way was used to perform the K-W analysis. Results were equivalent to the one-way ANOVA.

Number of observations in data set = 200
Tukey's Studentized Range (HSD) Test for variable: LTBD
Alpha= 0.1 df= 180 MSE= 0.615044
Critical Value of Studentized Range= 3.506
Minimum Significant Difference= 0.4347

Means with the same letter are not significantly different.

Tukey Grouping	Mean	N	TRTMNT
A	4.5895	40	t90300
B	3.9725	40	t110300
B			
B	3.9093	40	t90500
B			
C B	3.7590	40	t110500
C			
C	3.3992	40	Cntrl

Analysis of Variance
Class Level Information

Class	Levels	Values
VOLT	4	13 14 15 16
TEMPT	2	300 500
TEMPD	2	2.61 2.75

Number of observations in data set = 160
Dependent Variable: LTBD

Source	DF	Sum of Squares	Mean Square	F Value	Pr > F
Model	15	383.25900071	25.55060005	38.68	0.0001
Error	144	95.11130043	0.66049514		
Corrected Total	159	478.37030113			

R-Square	C.V.	Root MSE	LTBD Mean
0.801176	20.02943	0.8127085	4.0575713

Source	DF	Anova SS	Mean Square	F Value	Pr > F
VOLT	3	352.35607715	117.45202572	177.82	0.0001
TEMPT	1	7.98677830	7.98677830	12.09	0.0007
VOLT*TEMPT	3	0.97274241	0.32424747	0.49	0.6891
TEMPD	1	5.88696557	5.88696557	8.91	0.0033
VOLT*TEMPD	3	11.54149373	3.84716458	5.82	0.0009
TEMPT*TEMPD	1	2.17893673	2.17893673	3.30	0.0714
VOLT*TEMPT*TEMPD	3	2.33600681	0.77866894	1.18	0.3200

Figure 2: Annotated output from SAS procedure ANOVA

Stress-Life Model Estimation

To consider the fit of the average DC life for the thermally aged polypropylene films to semi-empirical single and multistress models [2], the sequential application of stress (thermal then electrical) can be modelled as having a simple additive effect. However, this approach is too simplistic and is not appropriate for our data since no unique trend was observed within the stress range tested. The single stress models (Exponential and Inverse Power) compare test groups as a function of the electrical stress only ignoring the quantitative aspect of the treatment variables. A multivariable model such as the multiplicative effects model is a better alternative, though may not be theoretically founded. Multiple Linear of first order and second order polynomial including interaction terms such as the General Eyring relationship. A more meaningful model is a nonlinear one that requires a large data set and a wider range of test conditions. The model is not fully developed and will not be discussed in this paper.

Regression (empirical curve-fitting) expresses the transformed response variable; ln(time-to-failure) as a function of the independent variables; applied stresses, plus a random part (error or natural variation in data). Methods for carrying out regression include: Least Squares, LSQ and Maximum Liklihood, ML; LSQ being the easiest to implement for complete Normally distributed data while the ML method is more versatile being valid for complete and censored data of any distribution. The ML estimates maximize the sample Likelihood (a product of the specimen liklihoods) w.r.t the parameters of the model. The Lifereg procedure in SAS, fits parametric models to failure time data with various possible distributions using ML methods. A *chi-square* test statistic is used to test the significance of the effect of each class variable on the response variable along with the Pr>Chi which should be less than α if the effect is significant. A Liklihood ratio test is used to test for the most significant model. Since a Lognormal distribution was determined to be valid for the data, LSQ methods suffice.

A check of many assumptions about the data is required for validity of inference with LSQ regression, yet is robust enough to allow minor deviations in practical applications. The LSQ estimates are obtained by minimizing the sum of squared difference between observed and predicted values, defined as the error sum of squares.

SAS procedure REG fits linear models using LSQ methods. An F statistic tests the overall significance of the model and the R^2 measures variation in the response variable due to the independent variables vs. error, i.e., a goodness of fit measure for the model. Optimum subsets of variables for best models are selected based on the R^2 and C(p) statistic [1]. Procedure RSREG (Response Surface regression) is used for testing the quadratic response surface model which includes second order powers and cross terms of the stress variables.

For Single Stress models, an Exponential/Lognormal model was found to be slightly more significant than other Power and Weibull models. It has be en noted in the literature that distinction between fit to these two models can only be achieved with very large data sets. Multiple-variable models had a higher R^2 value of up to 0.80 and thus are more appropriate. The contribution of quadratic terms to the model was found to be insignificant and were therefore not included in the final model. Only linear terms and two interaction terms increased the effectiveness of the model. No lack of fit was detected indicating an overall adequate model. Procedure REG was used to select the best five terms to be included in the model. The best model was determined to be the following:

$$tbd = \beta_0 . \exp(\beta_1 T') . \exp(\beta_2 \tau) . \exp(\beta_3 V) . \exp(T' . [\beta_4 V + \beta_5 \tau]) \qquad (1)$$

where, *tbd* is the time to breakdown, β_0, β_1, β_2, β_3, β_4, and β_5 are constants (coefficients of regression) and T '= [1000 / (273.2 + T(°C))], V is voltage in kV and τ is thermal stressing time in hours. Parameter values are given in Fig. (3). Plots of residuals vs. predicted response by the model verified the adequacy of the model and the homogeneity of the errors. Fig. (4) shows the predicted 3-D surface response of the model for each aging temperature.

Analysis of Variance

Source	DF	Sum of Squares	Mean Square	F Value	Prob>F
Model	5	369.09723	73.81945	104.035	0.0001
Error	154	109.27307	0.70957		
C Total	159	478.37030			

Root MSE	0.84236	R-square	0.7716
Dep Mean	4.05757	Adj R-sq	0.7642
C.V.	20.76013		

Parameter Estimates

Variable	DF	Parameter Estimate	Standard Error	T for H0: Parameter=0	Prob>|T|
INTRCPT($\ln\beta_0$)	1	-111.34299	34.70895641	-3.208	0.0016
VOLT(β_3)	1	6.281311	2.28121416	2.753	0.006
TEMPD(β_1)	1	50.501209	12.94668762	3.901	0.0001
TEMPT(β_2)	1	0.042444	0.02550475	1.664	0.0981
TEMPD*TEMPT(β_4)	1	-0.016671	0.00951345	-1.752	0.0817
VOLT*TEMPD(β_5)	1	-2.833968	0.85090911	-3.331	0.0011

Figure 3: Annotated output from SAS procedure REG

Diagnostics

A number of diagnostic tests were carried out to detect correlating chemical or physical changes in bulk or surface properties of the aged films. Results of FT-IR, X-ray diffraction, NMR and AFM did not reveal any significant differences. Spectra from ESCA, mapping present elements on the film surface to a depth of 50Å, detected the O_2 atomic % to be inversely related to the film lifetime. The Young's modulus also correlated with the lifetime trends.

Discussion and Conclusion

The inherent variability of the lifetimes of insulation systems necessitates the use of statistical methods to analyze the data and assure valid inference about the system. This paper has presented a multitude of such methods. Limitations of practical applications and time pose challenging constraints on the conduction and interpretation of aging studies.

For the range of aging temperatures tested, the lifetimes of the polypropylene films seem to be inversely related to increased temperature for equal treatment hours and increased number of hours at a given temperature. The trend correlates with the Oxygen (atomic %) on the film surface and Young's modulus values. A multiplicative effects model including interaction terms describes the stress-life behavior adequately.

Acknowledgement

This work was partially supported by BMDO/ONR #N00014-93-1-0483.

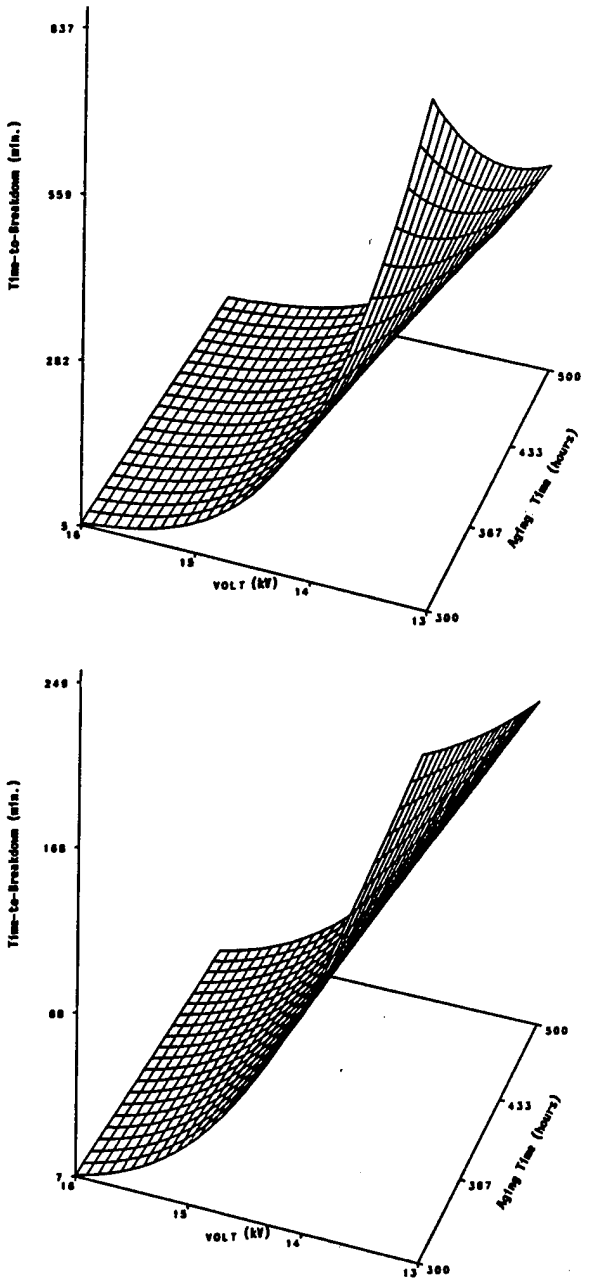

Figure 4: Lifetime Surface Response for aged PP films @ 90°C and 110°C

References

1- SAS Institute Inc. "SAS/STAT User's Guide, Version 6, Fourth Ed. Vol. 1&2, Cary NC:SAS Institute Inc. 1989.
2- W. Nelson, Accelerated Testing, John Wiley & Sons, NY 1990.
3- H. M. Wadsworth Jr., Editor, Handbook of Statistical Methods for Engineers and Scientists, McGraw Hill, NY 1990.
4- G. C. Stone, "Personal Statistical Package for the Extreme-Value and Weibull Distributions", 1978.

Conference Record of the 1994 IEEE International Symposium on Electrical Insulation, Pittsburgh, PA USA, June 5-8, 1994

TESTING OF CABLE INSULATION FOR AEROSPACE APPLICATIONS

A. N. Hammoud, M. W. Stavnes
NYMA, Inc.
Cleveland, OH 44130

J. L. Suthar, W. Khachen, and J. R. Laghari
Department of Electrical Engineering
State University of New York at Buffalo
Buffalo, New York 14260

Abstract

Reliable cable insulation is needed to replace MIL-W-81381 (polyimide) in low to medium voltage aerospace power applications. Potential cable insulation systems are tested to determine their suitability in an aerospace environment. The top ten cables insulations recommended by NASA Lewis Research Center (based on preliminary evaluation done by Air-Force Wright Laboratory (WL) and by NASA Johnson Space Center/White Sands Test Facility (WSTF)) are evaluated for their dielectric properties. Test results on electrical breakdown measurements made on the cables under dc, ac 60 Hz, and ac 400 Hz electric field at three temperatures: 23° C, 100° C, and 200° C in a circulating hot air environment are presented.

Introduction

Polyimide-based wiring insulation (MIL-W-81381) has been extensively used in aerospace power distribution systems because polyimide insulation is light weight and has good dielectric properties, including high service temperature and dielectric strength. However, if polyimide-insulated wires are abraised or mechanically damaged, resistive heating and arcing may occur causing the insulation to become conductive, leading to breakdown and failure of the electrical system.[1] The quality of cable insulation in most space vehicles is according to 1970's aerospace standards, and do not take into account arc-tracking, flashover and multistress aging.[2] A recent study reports that MIL-W-81381 cables, for example, have failed prematurely in a number of Air Force, Navy and NASA power systems due to intense arcing.[2,3] Therefore, it has become essential to characterize replacement aerospace cable insulations for their physical integrity and dielectric properties, such as dielectric strength, flashover, arc-tracking and multistress aging. A recent NASA workshop on wiring for space applications has addressed key technology issues on space wiring and proposed a number of alternate wiring insulation structures.[4] Some of these cable insulation systems have shown superior physical properties, such as better flexibility, good temperature capabilities and mechanical properties.[4,5] There was a need to evaluate the dielectric properties of these cables under high temperature conditions.

The present work evaluates the dielectric strength of ten cable insulation systems. These include MIL-W-81381, Gore, Tensolite, Filotex, and Teledyne cable insulation systems, each in two different gauges: 12 and 20 AWG. These wiring constructions are comprised of different combinations of insulation materials including Kapton, PTFE and TFE.[4] The insulation composition and thickness of each cable is provided in Table 1. Breakdown measurements were performed on these cables under dc, ac 60 Hz, and ac 400 Hz electric fields at three different temperatures: 23° C, 100° C, and 200° C in a circulating hot air environment. Because of similarities in the trend of the data obtained, i.e. no dependence of breakdown voltage on gauge size, only the results for the 12 AWG cable samples are reported. The experimental results which are presented allow a comparison of their dielectric performance in a high temperature environment.

Experimental Procedure

The high temperature testing facility is shown in Figure 1. A machineable high temperature ceramic was used to provide the high voltage feedthru inside the test chamber. High voltage was applied to the cable conductor, which was looped between two grounded electrodes (round edge plates). The circulation of hot air

Table 1: Cable Insulation Systems.

Sample	Insulation System	Insulation Thickness
M81381-12	Kapton with Polyimide top coat	8.6 mil
M81381-20	Kapton with Polyimide top coat	8.6 mil
Gore-12	PTFE/ High Strength PTFE/ PTFE	6 mil
Gore-20	PTFE/ High Strength PTFE/ PTFE	6 mil
Tensolite-12	PTFE/ Polyimide/ PTFE	7.15 mil
Tensolite-20	PTFE/ Polyimide/ PTFE	6.15 mil
Filotex-12	PTFE/ Polyimide/ FEP	6.9 mil
Filotex-20	PTFE/ Polyimide/ FEP	6.5 mil
Teledyne-12	PTFE/ Polyimide/ PTFE	6 mil
Teledyne-20	PTFE/ Polyimide/ PTFE	6 mil

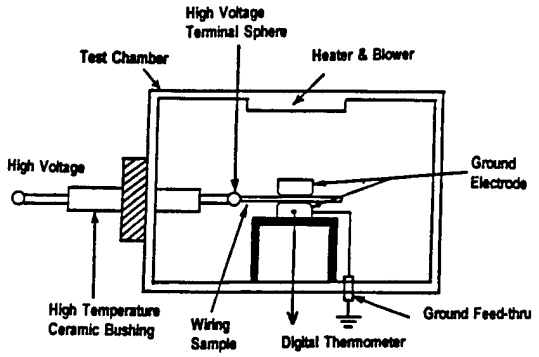

Figure 1 The High Temperature Testing Facility.

in the test chamber helped to maintain uniform thermal stresses to the cable sample being tested. The rate of rise of the voltage was 500 V/sec, which complied to ASTM D149, until breakdown occured. Each cable specimen was about twelve inches long. The entire surface of the sample was cleaned with heptene to minimize contamination of the surface due to handling. A ten minute time interval was allowed for each sample to reach the proper test temperature. Due to the statistical nature of the experimental results, seven replicate measurements were obtained for each breakdown voltage data point reported.

Results and Discussion

Breakdown voltages of the cable insulations are reported in figures 2 to 4 as a function of temperature. The value for breakdown voltages reported are an average of seven data points.

Figure 2 shows the dc breakdown voltages for all five cables as a function of temperature up to 200° C. It can be seen from the figure that MIL-W-81381 shows the highest dc breakdown strength whereas Gore gives the lowest values at all temperatures. It is apparent from the figure that the cable insulation, of any given sample, undergoes a slight decrease in their breakdown voltages at 200° C from their room temperature values. This reduction in the breakdown voltages at 200° C varies from as low as 2% for the MIL-W-81381, to as high as 14% for Teledyne.

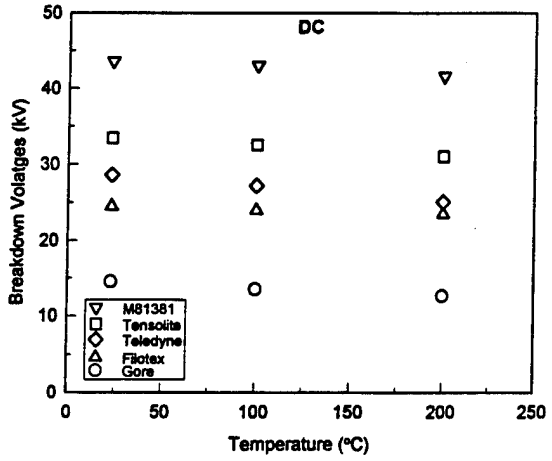

Figure 2 DC Breakdown Voltages of Cable Insulation Systems versus Temperature.

The dependence of ac 60 Hz breakdown voltage of the cable insulations on test temperatures is shown in Figure 3. The figure shows a similar trend of ac breakdown voltages up to 100° C. However, breakdown voltages decrease more rapidly when temperature is increased to 200° C. Such a reduction in ac breakdown strength can be attributed to an increased dielectric loss in insulating materials subjected to high temperatures.[6]

Breakdown voltages of insulation cables obtained at ac 400 Hz at three temperatures are shown in Figure 4. Except for the MIL-W-81381 construction, the cables did not undergo a significant reduction in their breakdown voltages when the test temperature was increased to 200° C. The breakdown voltages of MIL-W-81381 seems to be stable at temperatures up to 100° C, however, it experienced a 20% decrease when the temperature was further raised to 200° C at test frequency of 400 Hz.

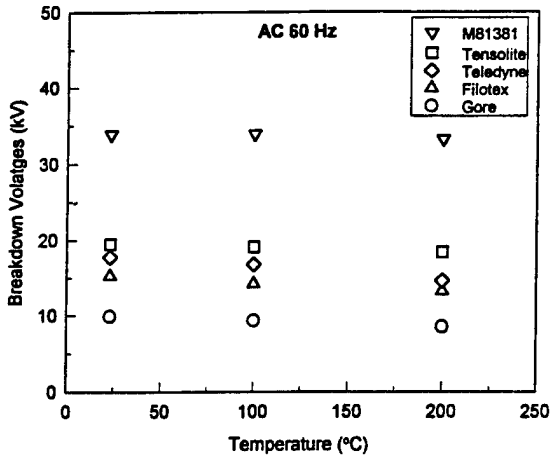

Figure 3 Temperature dependency of AC 60 Hz Breakdown Voltages (0-Peak).

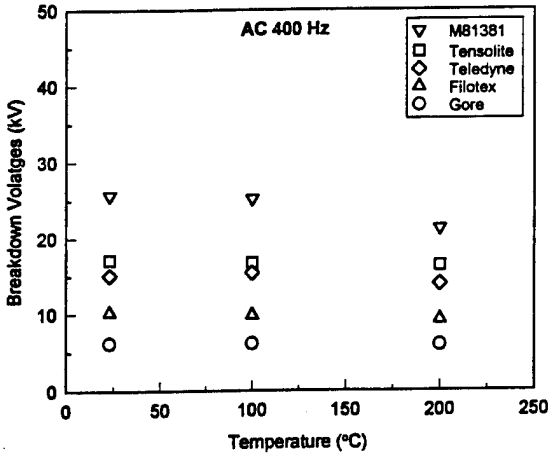

Figure 4 AC 400 Hz Breakdown Voltages (0-Peak) of Cable Insulation Systems versus Temperature.

The data presented in Figure 2 to 4 shows that all five cable insulations exhibit a reduction in their breakdown voltages to some degree at higher temperatures. Such negative temperature dependency of breakdown behavior can be attributed to the softening and degradation of the polymer at high temperatures.[7]

To visualize the effect of different electric fields on the breakdown phenomena in cable insulations, the results are illustrated as a function of applied voltage frequency in Figure 5. MIL-W-81381 shows the highest breakdown voltage among all the cables tested. Also, dc breakdown voltages of the cable samples are higher than ac breakdown voltages. This is probably because the space charge formation in insulating material under dc fields often lowers the local field by aligning the dipoles in opposite direction. A lower dielectric loss in the

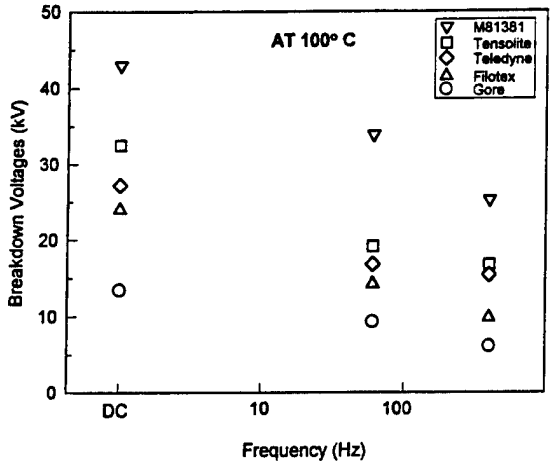

Figure 5 Breakdown Voltage of Cable insulation Systems under various applied Fields.

dielectrics under dc fields further improves the breakdown strength. On the other hand, higher dielectric loss of the material, due to higher temperatures and ac fields, often converts into additional joule heating and rapidly degrades the ac breakdown strength of the polymer dielectrics. Since the dielectric loss also characteristically depends on the frequency of the ac fields, the 400 Hz ac breakdown voltages are lower then ac 60 Hz, as shown in Figure 5.

Conclusion

In general, MIL-W-81381 (polyimide) cables, which are widely used in aerospace power systems, show the highest breakdown voltages at all temperatures and exhibit about a 20% reduction in their breakdown strength under extreme stresses (i.e. ac 400 Hz and 200° C). On the other hand, Teledyne, Filotex, Tensolite, and Gore cable insulations are capable of maintaining a stable breakdown strength over a wide range of temperatures despite their lower nominal voltages than the MIL-W-81381. Some of these cable insulations also possess superior physical properties, such as better flexibility, good temperature capability and mechanical properties. Additional dielectric tests, such as flashover, arc-tracking and multistress aging, are needed on the candidate cables to determine their reliability and suitability for aerospace applications.

Acknowledgement

This work was mainly supported by NASA LeRC, Cleveland, Ohio, under Grant number NAG-31345 and also partially supported by BMDO/ONR under Grant # N00014-93-1-0483.

REFERENCES

[1] R. W. Bercaw and R. C. Cull, "Electrical System Options for Space Exploration", 26th Intersociety Energy Conversion Engineering Conference, Boston, MA, August 1991.

[2] R. V. Peterson, "Orbiter Kapton Wire Operational Requirements and Experience", 1st NASA Workshop on Wiring for Aerospace Applications, NASA LeRC, Cleveland, OH, July 1991.

[3] F. J. Campbell, "Problems with Aging Wiring in Naval Aircraft", 1st NASA Workshop on Wiring for Aerospace Applications, NASA LeRC, Cleveland, OH, July 1991.

[4] R. Soloman, L. Woodford and S. Domalewski, "New Insulation Constructions for Aerospace Wiring Applications", Air Force Report # WL-TR-91-4066, June 1991.

[5] L. A. Burkhardt, "Electrical and Mechanical Testing of Wire Insulation for Space Applications", 2nd NASA Workshop on Wiring for Aerospace Applications, NASA LeRC, Cleveland, OH, October 1993.

[6] J. L. Suthar and J. R. Laghari, *"Breakdown Studies of Teflon Perfluoroalkoxy Film at High Temperature"*, Journal of Materials Science, Vol 27, pp 1795-1800, 1992.

[7] A. N. Hammoud, E. D. Baumann, E. Overton, I. T. Myers, J. L. Suthar, J. R. Laghari, and W. Khachen, "High Temperature Dielectric Properties of APICAL, Kapton, Teflon AF, and UPILEX Polymers" Annual Report, Conference on Electrical Insulation and Dielectric Phenomena, British Columbia, Canada, pp 549-554, October 1992.

Conference Record of the 1994 Twenty-First International Power Modulator Symposium, Costa Mesa, CA, June 27-30, 1994

Microdischarge Detection in High Frequency Capacitors

C. Nowak, J. Stopher, and J. Zirnheld
312 Bonner Hall
Department of Electrical and Computer Engineering
University at Buffalo, SUNY

and
R. Dollinger
Box 601900
Buffalo, NY 14260-1900

Abstract

Higher frequency power is playing an increasingly important role in the power conditioning and high power electronics areas. This is evident in many new applications of high frequency devices such as switching power supplies, radar modulators, and numerous pulsed power applications. Multi-factor stressing and related erosion of the dielectric material from microdischarges form a dominant cause of device failure, and this insulation deterioration can be accelerated under higher frequency stressing. The methods developed to investigate component failure have been established in the past by 60 Hz system requirements. Conventional detection systems are designed for dc, 60 Hz, and 400 Hz, but cannot generally be applied at high frequencies. This lack of high frequency diagnostic capabilities has contributed to a poor understanding of aging processes and failure mechanisms in new high frequency devices. To help researchers understand the fundamental aging processes and reliably be able to predict service lifetimes, new tools that can detect and analyze microdischarge activity under high frequency conditions are being developed.

This paper describes the design of a new microdischarge detection technique that can be used at high frequencies, and it's application to capacitors. This technique uses a series resonant multikilohertz power system in which the primary capacitance is two capacitors under test. Preliminary assessment of this new detection technique have validated its applicability to high frequency components. Initial test data and it's relevance will be discussed in detail.

This new detection technique offers a multi-spectral diagnostic capability which will help advance scientific understanding of the fundamental aging processes under the high frequency conditions for which the devices are designed.

Introduction

It can be argued that most general system failures are likely to be the result of an insulation breakdown in some manner. A capacitor specifically is an insulation device designed to withstand voltages, and many times capacitors are operated in regimes where their response is not completely understood, but merely inferred. Rep-rate high frequency is becoming increasingly important as a new operational area, and there is no technique in existence[1] that can adequately test the effects of high frequencies and the ensuing microelectrical discharges on capacitors. To this end, a new system has been developed with numerous potential diagnostic capabilities[2]. Of specific interest are it's unique power supply, detection method, and flexibility for high frequency device level testing.

This work was partially supported by BMDO/ONR grant # N00014-93-1-0483

Although these new topics will be covered in detail, a brief discussion of conventional discharge detection technology will first be presented as a background comparison.

Power supplies for low frequency testing is usually achieved by direct transformer action. The source must be designed to be microdischarge and corona free. The low frequency charging of capacitive test samples allows for low power requirements.

Microdischarge detection schemes designed for 60 or 400 Hz testing are readily available. The conventional filter and detection technique used in these systems is usually a capacitive voltage divider, followed by an LCR circuit that is shock excited by discharges from within the test sample. The LCR circuit is a detection impedance designed specifically for the microdischarge frequency. This arrangement results in the output of a single voltage pulse proportional in magnitude to the size of discharge. Although the filtering technique of this conventional system works well at low frequencies, it is not suitable for higher frequencies. As the test frequency increases, the voltage drop across the detection impedance increases as well. As a result, test voltage appears on the output with the discharge signal and reduces the system's sensitivity to low level discharges. This conventional arrangement is sufficient for frequencies under 2 kHz.[3]

Design and Detection

Test Facility

The test facility, shown in Figure 1, is comprised of a series resonant power supply, bridge-type test fixture, detection transformer, filter, shielding, fault protection, measurement apparatus, and calibration circuitry.

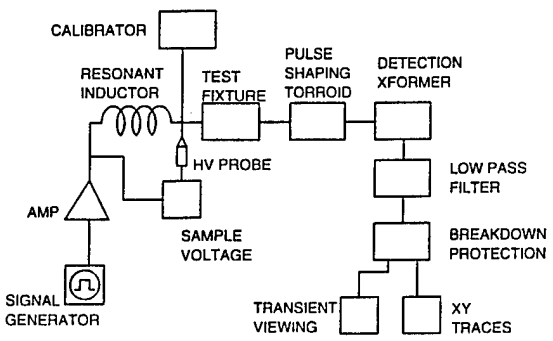

Figure 1. Major components of facility.

High Voltage Supply

A series resonant technique was employed to generate the partial discharge free high voltage across the capacitor test objects. This voltage is steady-state sinusoidal ac, with test frequencies between 2 kHz and 100 kHz. Series resonance was achieved using the capacitance value of the capacitors under test, a hand wound air core inductor, an audio amplifier, and a signal generator. Series resonance provides several desirable characteristics. In the event of sample failure, the test capacitance changes sufficiently to drop the system out of resonance, decrease peak voltages, and limit the amount of energy available. This also has the effect of decreasing current draw off-resonance, which allows easy control while adjusting test frequency.

A Hewlett-Packard 651B test oscillator and a 100 watt (~ 90 Vpp) with 50 Ω output impedance was used to generate the applied test voltage. The primary inductance used for resonance was provided by either single layer hand wound air core inductors, which ranged from 40 μH to 60 mH, or by commercially wound components such as a Brooks coil (5H) or other power transformer secondaries (~2H). The available inductors, together with typical test object capacitances on the order of 2000 pF, provided resonance test frequencies between 2 kHz through 100 kHz by virtue of the following equation;

$$\omega_o = \frac{1}{\sqrt{LC}} \qquad [1]$$

The available resonant frequencies actually went well beyond 1 MHz, however the response of the audio amplifier dropped off above 100 kHz.

A Gentec 10,000:1 20 kV partial discharge free high voltage probe was used to observe the test specimen voltage. This capacitive probe has less than 20 pF and did not significantly load the specimen. While the specimen voltage was monitored at low voltage, the signal generator was manually adjusted until resonance was observed by a peak rise in voltage. The peak voltage can be estimated by multiplying the applied voltage and the quality factor Q of the series resonant circuit, given by;

$$Q = \frac{\sqrt{L/C}}{R} \qquad [2]$$

The inductors, capacitance, and amplifier used provided a Q on the order of 25, and generated test voltages near 2.5 kV.

Test Fixture

The test fixture, illustrated in Figures 2,3, and 4 provide the basis for allowing high frequency microdischarge detection. It consists of two specimen cells, a pulse shaping toroid, a detection transformer, and a damping resistor.

The two pairs of 2" diameter brass electrodes conform to ANSI standards. Both test capacitors are charged simultaneously. The charging current travels through each branch of the pulse shaping toroid, through the detection transformer primary, out the center tap, and back to the power supply.

The winding sense around both toroids in each branch of the test fixture is counter with respect to each other. This opposing sense reduces the inductance and subsequently provides a minimum impedance path for charging. More importantly, a minimum net flux is generated within the transformer core, and therefore, minimum output noise is generated at the secondary. In fact, if the currents in each branch are equal, and the number of turns about each branch of the transformer is equal, then there should be zero output, regardless of frequency or voltage. The N*I magnetomotive forces which generate the flux are illustrated in Figure 3. Note that this effect (minimum voltage out) is true for charging currents (common mode currents), but there is an opposite effect (maximum voltage out) for a current originating within a capacitor sample (differential or circulating current). This circulating current is the result of a discharge within a capacitor under test. This is an important distinction, and the heart of this detection technique.

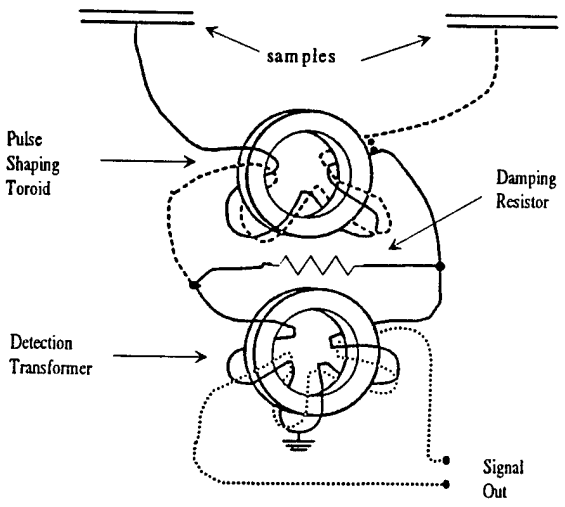

Figure 2. High frequency bridge type test fixture.

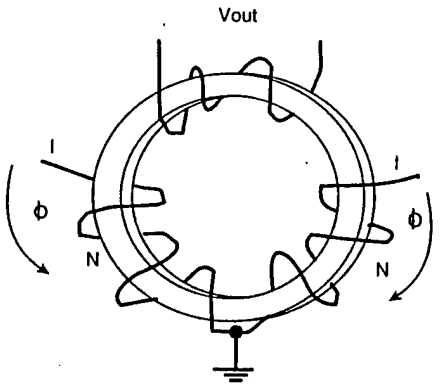

*Figure 3. N*I magnetomotive forces that generate core flux which creates the output at the secondary.*

Discharge Event

During a discharge, the voltage generated by charge recombination distributes itself around the path of the test fixture, primarily by inductive distribution. The resulting current flow is confined to within the test fixture and circulates through the detection transformer.

This effect is assured because the test fixture impedance is small compared to that of the resonant inductor and power supply. Initially, the current will flow until the charge on both specimens distributes evenly. The resulting transient response is a critically damped single pulse waveform caused by the parallel RLC network of the fixture. Control of the pulse shape and duration is accomplished by changing the inductance of the pulse shaping toroid and the damping resistor.

It was stated that a discharge event in a capacitor will generate a maximum voltage at the secondary of the output transformer. This is a subtle yet paramount point of the system. This discharge and resultant current will circulate around the test fixture in a specific manner, enabling it to be viewed with standard diagnostic equipment. In this way, the discharge itself can be seen at high frequencies with no swamping effect from the high voltage. More so, the direction of the circulating current distinctly determines which capacitor is discharging. Figure 4 illustrates the difference between the charging current (common mode, dashed line) and the discharge current (differential mode, dotted line). The discharging capacitor can be determined by viewing it's discharge trace. A convention has been adopted which indicates the discharging capacitor. If a positive rising edge discharge is present with a positive applied voltage, it is originating in the RED test cell of Figure 4. The BLACK cell generates a negative rising edge discharge on a positive applied voltage. This has been experimentally verified by intentionally inducing discharges in a specific cell through selective field enhancement. Figure 5 shows a positive discharge on a positive applied voltage and also a negative discharge on a negative applied voltage, indicating the RED test cell.

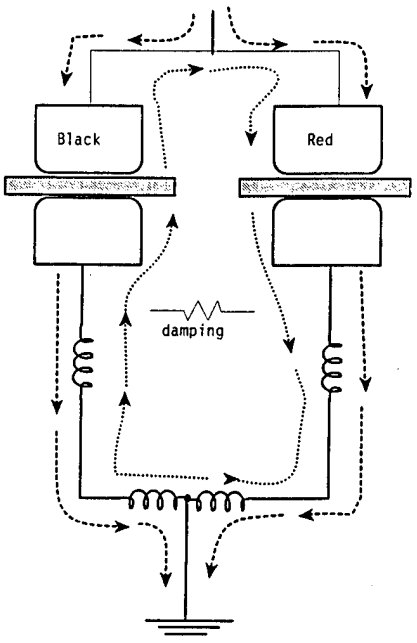

Figure 4. *Test fixture charging current (dashed line) and discharge current (dotted line).*

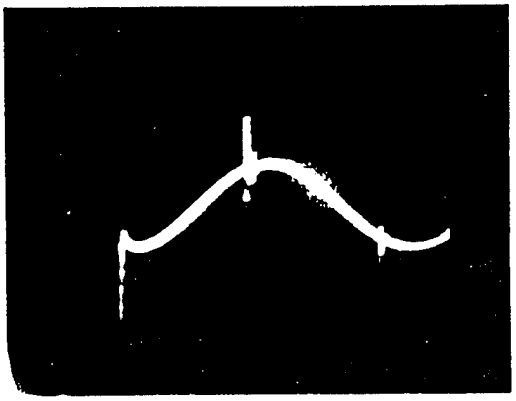

Figure 5. *Positive discharge rising edge on positive applied voltage, indicating RED cell discharge.*

Measurement Results

Two types of capacitors have been tested, a 1000 pF 400 V dc polyester, and a 4700 pF 1 kV mica. The 400 V dc polyester capacitor was tested at 14 kHz. Figure 6 shows XY traces of polyester without and with discharge activity at 1000 Vpp and 1200 Vpp, respectively. The Y axis is microdischarge activity and the high voltage is X axis (with the highest positive voltage to the right and the highest negative voltage to the left). Note the increased activity at the higher voltage. Also note that the negative discharge activity on positive applied voltage (negative bump near right end) and positive activity on negative applied voltage (positive bump near left end). This specific relationship of activity indicates that the BLACK cell capacitor experienced more discharge than the RED cell capacitor and is polarity insensitive.

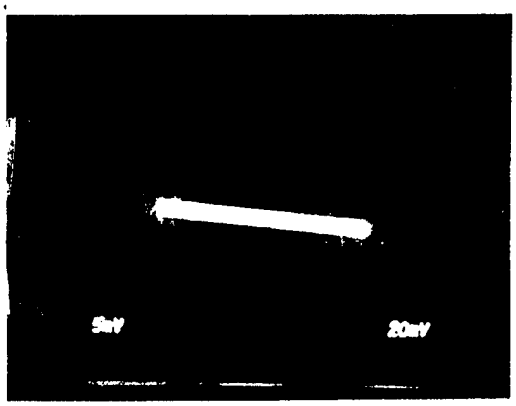

Figure 6a. *Two each 1000 pF, 400 V dc polyester capacitor at 14 kHz and 1000 Vpp (no discharges).*

254

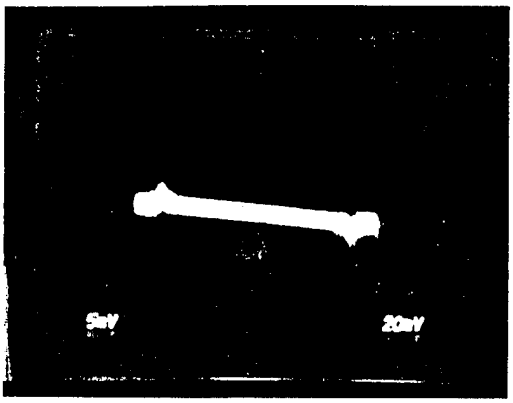

Figure 6b. Two each 1000 pF, 400 V dc polyester capacitor at 14 kHz and 1200 Vpp (with microdischarges).

Figure 7 shows 5 kHz discharge activity for mica at 800 Vpp and 1250 Vpp. Note that the discharge activity began at only 80% of the dc rated voltage. Again, discharge activity seems to occur primarily in one capacitor. In contrast to Figure 6 for polyester the negative bump is at the left end and the positive is near the right end. Thus, one can see that discharge is occurring in the RED cell this time. Additionally, the discharges are more evenly spaced around the voltage cycle. Lastly, note the slant of the trace. A larger slant of Figure 6 than Figure 7 is indicative of more common mode "noise", which comes from less matched capacitors (and not from frequency differences, as shown by testing). Therefore, the mica capacitors are better matched than the polyester capacitors.

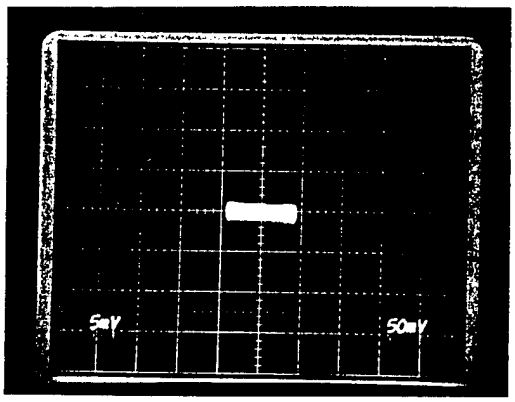

Figure 7a. Two each 4700 pF, 1 kV, mica capacitor at 5 kHz and 800 Vpp (no microdischarges).

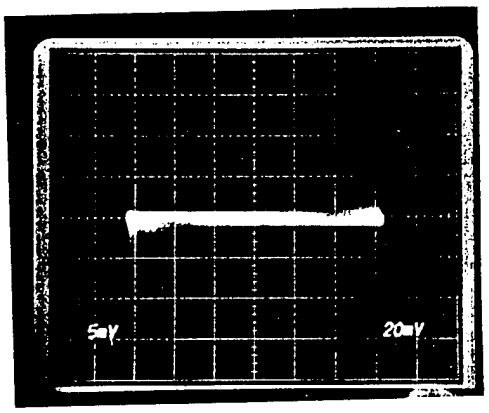

Figure 7b. Two each 4700 pF, 1 kV, mica capacitor at 5 kHz and 1250 Vpp (with microdischarges).

Conclusion

A new technique to perform device level testing at high frequencies has been developed. The major difference between this and former techniques is the ability to actually apply simultaneous high frequency, high voltage stress on a capacitor, and then view the microelectric discharges that precede device failure. This facility can currently test from 3 kHz to 100 kHz, and from 0 - 2000 Vpp. Ongoing work includes[4] determination of ideal capacitors for high frequency and voltage applications, and how the aging rate changes as capacitors are subject to these stresses.

References

[1] Dunbar, W.G., "High Frequency Electronics Partial Discharge Detection Needs." IEEE Annual Report, Conference on Electrical Insulation and Dielectric Phenomena, 1987.

[2] Stopher, J.P., "A New and Novel High Frequency Electrical Insulation Stressing and Microdischarge Detection Technique." Ph.D. Dissertation, Department of Electrical and Computer Engineering, University at Buffalo, SUNY, Buffalo, NY, 1994.

[3] ASTM D1868-87, "Standard Method for Detection and Measurement of Partial Discharge (Corona) Pulses in Evaluation of Insulation Systems." 1987 Annual Book of ASTM Standards, Vol. 10.02, ASTM Philadelphia, PA, 1987.

[4] Nowak, C.S., "The Role of Partial Discharges as a Failure Mechanism in High Frequency Applications of Capacitors." Ph.D Dissertation not yet published, Department of Electrical and Computer Engineering, University at Buffalo, SUNY, Buffalo, NY.

OFFICE OF THE UNDER SECRETARY OF DEFENSE (ACQUISITION)
DEFENSE TECHNICAL INFORMATION CENTER
CAMERON STATION
ALEXANDRIA, VIRGINIA 22304-6145

IN REPLY REFER TO DTIC-OCC

SUBJECT: Distribution Statements on Technical Documents

TO: OFFICE OF NAVAL RESEARCH
CORPORATE PROGRAMS DIVISION
ONR 353
800 NORTH QUINCY STREET
ARLINGTON, VA 22217-5660

1995 1027 005

1. Reference: DoD Directive 5230.24, Distribution Statements on Technical Documents, 18 Mar 87.

2. The Defense Technical Information Center received the enclosed report (referenced below) which is not marked in accordance with the above reference.

2ND ANNUAL REPORT
N00014-93-1-0483
TITLE: HIGH POWER ELECTRONICS INSTITUTE

3. We request the appropriate distribution statement be assigned and the report returned to DTIC within 5 working days.

4. Approved distribution statements are listed on the reverse of this letter. If you have any questions regarding these statements, call DTIC's Cataloging Branch, (703) 274-6837.

FOR THE ADMINISTRATOR:

1 Encl

GOPALAKRISHNAN NAIR
Chief, Cataloging Branch

FL-171
Jul 93

DISTRIBUTION STATEMENT A:

APPROVED FOR PUBLIC RELEASE: DISTRIBUTION IS UNLIMITED

DISTRIBUTION STATEMENT B:

DISTRIBUTION AUTHORIZED TO U.S. GOVERNMENT AGENCIES ONLY; (Indicate Reason and Date Below). OTHER REQUESTS FOR THIS DOCUMENT SHALL BE REFERRED TO (Indicate Controlling DoD Office Below).

DISTRIBUTION STATEMENT C:

DISTRIBUTION AUTHORIZED TO U.S. GOVERNMENT AGENCIES AND THEIR CONTRACTORS; (Indicate Reason and Date Below). OTHER REQUESTS FOR THIS DOCUMENT SHALL BE REFERRED TO (Indicate Controlling DoD Office Below).

DISTRIBUTION STATEMENT D:

DISTRIBUTION AUTHORIZED TO DOD AND U.S. DOD CONTRACTORS ONLY; (Indicate Reason and Date Below). OTHER REQUESTS SHALL BE REFERRED TO (Indicate Controlling DoD Office Below).

DISTRIBUTION STATEMENT E:

DISTRIBUTION AUTHORIZED TO DOD COMPONENTS ONLY; (Indicate Reason and Date Below). OTHER REQUESTS SHALL BE REFERRED TO (Indicate Controlling DoD Office Below).

DISTRIBUTION STATEMENT F:

FURTHER DISSEMINATION ONLY AS DIRECTED BY (Indicate Controlling DoD Office and Date Below) or HIGHER DOD AUTHORITY.

DISTRIBUTION STATEMENT X:

DISTRIBUTION AUTHORIZED TO U.S. GOVERNMENT AGENCIES AND PRIVATE INDIVIDUALS OR ENTERPRISES ELIGIBLE TO OBTAIN EXPORT-CONTROLLED TECHNICAL DATA IN ACCORDANCE WITH DOD DIRECTIVE 5230.25, WITHHOLDING OF UNCLASSIFIED TECHNICAL DATA FROM PUBLIC DISCLOSURE, 6 Nov 1984 (Indicate date of determination). CONTROLLING DOD OFFICE IS (Indicate Controlling DoD Office).

The cited documents has been reviewed by competent authority and the following distribution statement is hereby authorized.

A
(Statement)

OFFICE OF NAVAL RESEARCH
CORPORATE PROGRAMS DIVISION
ONR 353
800 NORTH QUINCY STREET
ARLINGTON, VA 22217-5660

(Controlling DoD Office Name)

(Reason)

DEBRA T. HUGHES
DEPUTY DIRECTOR
CORPORATE PROGRAMS OFFICE
(Signature & Typed Name)

(Assigning Office)

(Controlling DoD Office Address, City, State, Zip)

19 SEP 1995
(Date Statement Assigned)